# Drag reduction in homogeneous turbulence by scale-dependent effective viscosity

Roberto Benzi,[1,2] Emily S. C. Ching,[2] and Itamar Procaccia[2,3]
[1]*Dipartimento di Fisica and INFM, Università "Tor Vergata," Via della Ricerca Scientifica 1, I-00133 Roma, Italy*
[2]*Department of Physics, The Chinese University of Hong Kong, Shatin, Hong Kong*
[3]*Department of Chemical Physics, The Weizmann Institute of Science, Rehovot, 76100 Israel*
(Received 6 January 2004; published 13 August 2004)

We demonstrate, by using suitable shell models, that drag reduction in homogeneous turbulence is usefully discussed in terms of a scale-dependent effective viscosity. The essence of the phenomenon of drag reduction found in models that couple the velocity field to the polymers can be recaptured by an "equivalent" equation of motion for the velocity field alone, with a judiciously chosen scale-dependent effective viscosity that succinctly summarizes the important aspects of the interaction between the velocity and the polymer fields. Finally, we clarify the differences between drag reduction in homogeneous and in wall bounded flows.

DOI: 10.1103/PhysRevE.70.026304 PACS number(s): 47.27.Nz, 47.27.Ak

## I. INTRODUCTION

The addition of long chained polymers to turbulent flows can result in a significant reduction in the drag [1–4]. The phenomenon was discovered in 1949 [5] and has since attracted much attention, with most of the experimental literature reviewed and systematized by Virk [3]; the amount of drag reduction depends on the characteristics of the polymer and its concentration, but cannot exceed an asymptote known as the "maximum drag reduction" (MDR) curve which is independent of the concentration of the polymer or its characteristics. Recently, there is significant progress in the understanding of this phenomenon. A first step in forming an understanding was performing direct numerical simulations of model equations of viscoelastic flows, both in wall bounded and in homogeneous turbulence [6–8]. The Oldroyd-B and the finitely extensible nonlinear elastic-Peterlin (FENE-P) models first, and then simplified models like shell models and Burgers-like models [9–11], all exhibited drag reduction as a result of including the interaction between the velocity field and a second field representing the polymer (end-to-end) conformation tensor, see Figs. 1 and 2. In homogeneous turbulence, drag reduction is manifested as an increase in the root-mean-square (rms) velocity fluctuations at scales larger than the Lumley scale, which is defined as the scale at which the eddy turnover time is of the order of the polymer relaxation time. The intermediate scale rms energy fluctuations are suppressed due to a transfer of energy to the polymers. In wall bounded turbulence, drag reduction entails an increase in the mean velocity for a given pressure head, see Fig. 1. Here the Reynolds stress at the intermediate scales is suppressed [12]. We will argue, however, that there is a difference between the increase in the rms velocity fluctuations at large scales in homogeneous flows and the increase in the mean velocity in wall bounded flows: the former disappears when the system size goes to infinity (for a fixed Lumley scale) whereas in the latter case, an increase in the mean velocity near the wall (small and intermediate scales) does not disappear with an increase in the system size. This difference is fundamental to the different symmetries at play, the Galilean invariance in the case of the wall bounded flow versus translational invariance in the case of homogeneous flows. Nevertheless, we will argue later that the two cases can be discussed in similar physical terms. In a recent paper [13], it was shown that drag reduction in wall bounded flows can be conveniently discussed in terms of a "scale-dependent" effective viscosity. The aim of the present paper is to demonstrate that this notion is also useful in the context of homogeneous turbulence. In doing so we aim at simplifying the theoretical description, eliminating the explicit presence of a second field in the equations of motion, leaving the velocity field alone. The eliminated field, which represents the conformation tensor of the polymers, remains only as an effective viscosity in the equation of motion. Needless to say, this effective viscosity cannot be a number, since the amount of energy transferred from the velocity field to the polymer is strongly scale dependent; in homogeneous turbulence this transfer reaches a maximum near the Lumley scale. In wall bounded flows the degree of interaction between the polymers and the velocity field is a strong function of the distance from the wall, and so is the effective viscosity. Of course, in a full theory a scale-dependent scalar viscosity is not sufficient either, due to the anisotropy of the

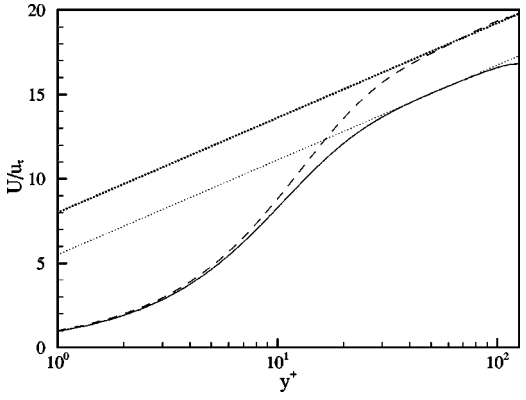


FIG. 1. Mean velocity profile of the FENE-P (dashed line) and of the Navier-Stokes equations (solid line) in wall bounded channel flow as a function of the reduced distance from the wall. The relative increase of the mean velocity (indicated by the asymptotic straight lines) is the phenomenon of drag reduction in wall bounded flows.

 

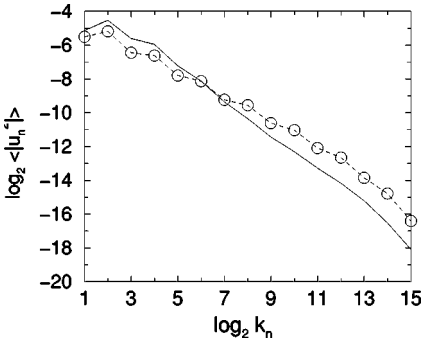


FIG. 2. Energy spectrum of the Sabra shell model with polymer (line) and the Sabra model without polymers (dashed line with symbols) for $\nu_s=10^{-7}$. The relative increase of the energy spectrum at small values of $n$ is the phenomenon of drag reduction in homogeneous turbulence in general and in shell models in particular, see Sec. III for details.

polymer end-to-end extension tensor. We would like to demonstrate, however, that at least in the model equations, a surprising proportion of the essential physics can be captured in terms of the simple notion of a scale-dependent viscosity which surrogates the existence of the second field. This thinking goes back to some observations a few years ago regarding the importance of space-dependent viscosity even in the stability of laminar flows [14,15]. In Sec. II we review the two-field models in which drag reduction was demonstrated in numerical simulations. In Sec. III we present the reduction to velocity-alone models with scale-dependent viscosity. In Sec. IV we present a discussion of the large system size limit and underline the difference between homogeneous and wall bounded flows. Section V is dedicated to a short summary and conclusions.

## II. SHELL MODEL FOR DRAG REDUCTION IN HOMOGENEOUS TURBULENCE

Viscoelastic flows are represented well by hydrodynamic equations in which the effect of the polymer enters in the form of a "conformation tensor" $\boldsymbol{R}(\boldsymbol{r},t)$ which stems from the ensemble average of the dyadic product of the end-to-end distance of the polymer chains [16–19]. A successful model that had been employed frequently in numerical simulations of turbulent channel flows is the FENE-P model. Flexibility and finite extensibility of the polymer chains are reflected by the relaxation time $\tau$ and the Peterlin function $P(\boldsymbol{r},t)$, which appear in the equation of motion for $\boldsymbol{R}$:

$$\frac{\partial R_{\alpha\beta}}{\partial t}+(\boldsymbol{u}\cdot\boldsymbol{\nabla})R_{\alpha\beta}=\frac{\partial u_\alpha}{\partial r_\gamma}R_{\gamma\beta}+R_{\alpha\gamma}\frac{\partial u_\beta}{\partial r_\gamma}-\frac{1}{\tau}[P(\boldsymbol{r},t)R_{\alpha\beta}-\rho_0^2\delta_{\alpha\beta}], \tag{1}$$

$$P(\boldsymbol{r},t)=(\rho_m^2-\rho_0^2)/(\rho_m^2-R_{\gamma\gamma}). \tag{2}$$

In these equations $\rho_m^2$ and $\rho_0^2$ refer to the maximal and the equilibrium values of the trace $R_{\gamma\gamma}$. Since in most applications $\rho_m \gg \rho_0$ the Peterlin function can also be written approximately as $P(\boldsymbol{r},t)\approx 1/(1-\alpha R_{\gamma\gamma})$ where $\alpha=\rho_m^{-2}$. In its turn the conformation tensor appears in the equations for the fluid velocity $\boldsymbol{u}(\boldsymbol{r},t)$ as an additional stress tensor

$$\frac{\partial \boldsymbol{u}}{\partial t}+(\boldsymbol{u}\cdot\boldsymbol{\nabla})\boldsymbol{u}=-\boldsymbol{\nabla}p+\nu_s\nabla^2\boldsymbol{u}+\boldsymbol{\nabla}\cdot\boldsymbol{\mathcal{T}}+\boldsymbol{F}, \tag{3}$$

$$\boldsymbol{\mathcal{T}}(\boldsymbol{r},t)=\frac{\nu_p}{\tau}\left[\frac{P(\boldsymbol{r},t)}{\rho_0^2}\boldsymbol{R}(\boldsymbol{r},t)-\boldsymbol{1}\right]. \tag{4}$$

Here $\nu_s$ is the kinematic viscosity of the neat fluid, $\boldsymbol{F}$ is the forcing, and $\nu_p$ is a viscosity parameter which is related to the concentration of the polymer, i.e., $\nu_p/\nu_s\sim\Phi$ where $\Phi$ is the volume fraction of the polymer. We note, however, that the tensor field can be rescaled to get rid of the parameter $\rho_m^2$ in the Peterlin function, $\tilde{R}_{\alpha\beta}=\alpha R_{\alpha\beta}$ with the only consequence of rescaling the parameter $\rho_0$ accordingly. Thus, the actual value of the concentration is open to calibration against the experimental data. These equations were simulated on the computer in a channel or pipe geometry, reproducing faithfully the characteristics of drag reduction found in experiments. It should be pointed out, however, that even for present day computers simulating these equations is quite tasking. It makes sense therefore to try to model these equations further. For the purpose of studying drag reduction in homogeneous systems, one can derive a shell model whose simplicity and transparency are assets for analysis and simulations alike. In developing a simple model one is led by the following ideas. First, it should be pointed out that all the nonlinear terms involving the tensor field $\boldsymbol{R}(\boldsymbol{r},t)$ can be reproduced by writing an equation of motion for a vector field $\boldsymbol{B}(\boldsymbol{r},t)$, and interpreting $R_{\alpha\beta}$ as the dyadic product $B_\alpha B_\beta$. The relaxation terms with the Peterlin function are not automatically reproduced this way, and one needs to add them by hand. Second, we should keep in mind that the earlier equations exhibit a generalized energy which is the sum of the fluid kinetic energy and the polymer free energy. Led by these consideration the following shell model was proposed in Refs. [9,11]:

$$\frac{du_n}{dt}=\frac{i}{3}\Phi_n(u,u)-\frac{i}{3}\frac{\nu_p}{\tau}P(B)\Phi_n(B,B)-\nu_s k_n^2 u_n+F_n,$$

$$\frac{dB_n}{dt}=\frac{i}{3}\Phi_n(u,B)-\frac{i}{3}\Phi_n(B,u)-\frac{1}{\tau}P(B)B_n-\nu_B k_n^2 B_n,$$

$$P(B)=\frac{1}{1-\Sigma_n B_n^* B_n}. \tag{5}$$

In these equations $u_n$ and $B_n$ stand for the Fourier amplitudes $u(k_n)$ and $B(k_n)$ of the two respective vector fields, but as usual in shell model we take $n=0,1,2,\ldots$ and the wave vectors are limited to the set $k_n=2^n$. The parameter $\nu_B=0.1\nu_s$ is an artificial viscosity needed to avoid the development of unphysical singularities in the system. The nonlinear interaction terms take the explicit form

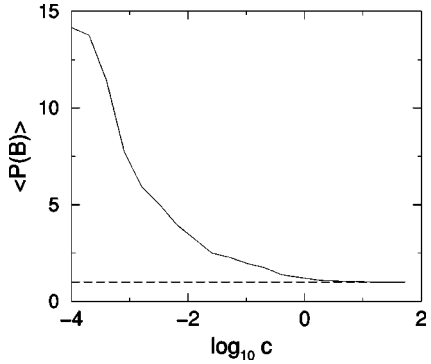


FIG. 3. The average value of the Peterlin function $P(B)$ as a function of $c$ computed in the SabraP model. The dashed line corresponds to $P=1$.

$$\Phi_n(u,B) = k_n[(1-b)u_{n+2}B^*_{n+1} + (2+b)u^*_{n+1}B_{n+2}] + k_{n-1}[(2b + 1)u^*_{n-1}B_{n+1} - (1-b)u_{n+1}B^*_{n-1}] + k_{n-2}[(2 + b)u_{n-1}B_{n-2} + (2b+1)u_{n-2}B_{n-1}], \quad (6)$$

with $b$ as a parameter and the obvious extension to $\Phi_n(u,u)$, $\Phi_n(B,u)$ and $\Phi_n(B,B)$. In accordance with the generalized energy of the FENE-P model [18,19], our shell model also has the total energy

$$E \equiv \frac{1}{2}\sum_n |u_n|^2 - \frac{1}{2}\frac{\nu_p}{\tau}\ln\left(1 - \sum_n |B_n|^2\right). \quad (7)$$

The second term in the generalized energy contributes to the dissipation a positive definite term of the form $(\nu_p/\tau^2)P^2(B)\Sigma_n|B_n|^2$. With $\nu_p=0$ the first of Eqs. (5) reduces to the well-studied Sabra model of Newtonian turbulence. We therefore refer the model with $\nu_p \neq 0$ as the SabraP model. As in the FENE-P case we consider $c \equiv \nu_p/\nu_s$ to be proportional to the concentration of polymers. In Ref. [9] it was shown that this shell model exhibits drag reduction, and the mechanism for the phenomenon was elucidated. Furthermore, it was shown in Ref. [11] that for large enough concentration, the Peterlin function can be disregarded (i.e, $P \approx 1$) and, consequently, the dynamics of the system becomes concentration independent, i.e., we reach the MDR asymptote. This behavior of the Peterlin function is shown in Fig. 3. Following this finding, we consider below the limiting case in which the concentration is large enough for the Peterlin function to be close to unity, $P \approx 1$. Finally, all the numerical simulations reported in this paper have been performed by using $b=-0.2$, $\nu_s=10^{-7}$, and a constant energy input given by

$$F_n = \frac{10^{-3}}{u^*_n} \quad (8)$$

for $n=1,2$ and $F_n=0$ for $n>2$. We remark that for different values of $b$ one obtains the same *qualitative* (but not quantitative) results, which we shall describe later. A constant energy input is chosen in order to provide clear evidence of drag reduction: for the same energy input, drag reduction is observed as an increase in the total kinetic energy of the flow.

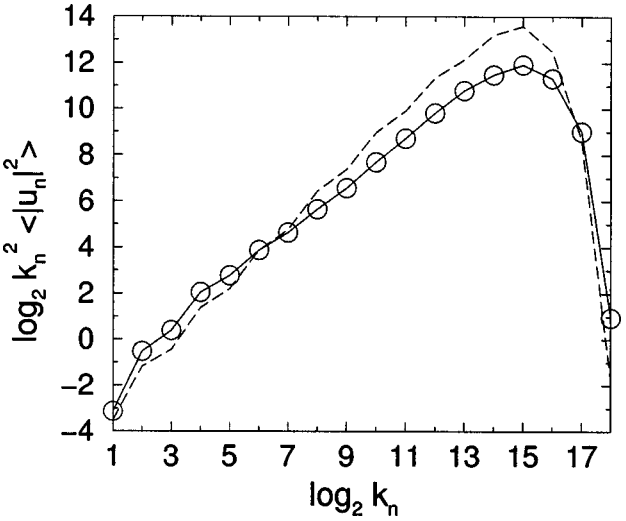


FIG. 4. The spectrum of the energy dissipation $k_n^2 e(k_n)$ for the Sabra (solid line with symbol) and the SabraP models (dashed line). Both models have a maximum at $k_n$ with $n \sim 15$, which corresponds to the peak in the energy dissipation.

## III. SCALE DEPENDENT EFFECTIVE VISCOSITY IN HOMOGENEOUS DRAG REDUCTION

Drag reduction in homogeneous turbulence is manifested as a relative increase in the rms fluctuations of the energy at large scales. We thus focus naturally on the energy spectrum $e(k_n) \equiv \langle u_n u_n^* \rangle$. In the context of the shell model the phenomenon is demonstrated in Fig. 2 where $e(k_n)$ is shown for the given values of the parameters. The spectra for the Sabra model (line with symbols) and the coupled SabraP model (line) are compared for the same amount of power input per unit time. The discussion of the spectra revolves around the typical Lumley scale $k_c$ which is determined by the condition

$$e^{1/2}(k_c)k_c \approx \tau^{-1}\langle P(B)\rangle. \quad (9)$$

For $k_n \gg k_c$ the decay time $\tau$ becomes irrelevant for the dynamics of $B_n$. The nonlinear interaction between $u_n$ and $B_n$ at these scales results in both of them having, theoretically, the same spectral exponent which is also the same as that of the Sabra model. The amplitude of the $u_n$ spectrum in the SabraP model is, however, smaller than that of the Sabra model since the $B_n$ field adds to the dissipation. On the other hand, for $k_n \ll k_c$, the $B_n$ field is exponentially suppressed by its decay with relaxation time $\tau$, and the spectral exponent of $u_n$ is again as in the Sabra model. Drag reduction comes about due to the interactions of the $u_n$ and $B_n$ fields at length scales of the order of $k_c$, which force a strong tilt in the $u_n$ spectrum there, causing it to cross the Sabra spectrum, leading to an increase in the amplitude of the energy containing scales. This is why the kinetic energy is increased for the same amount of power input, and hence, drag reduction. A complete theoretical discussion is presented in Ref. [9]. In Fig. 4, we show the spectrum of energy dissipation $k_n^2 e(k_n)$. This

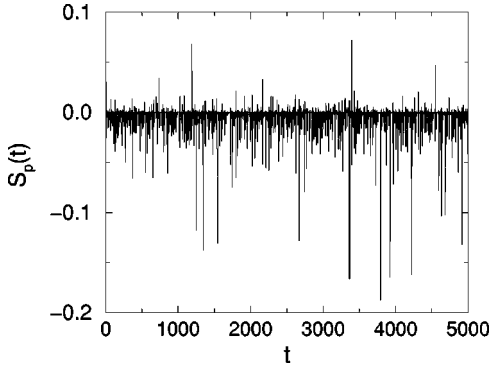


FIG. 5. Time behavior of $S_p$, as defined in Eq. (10), which represents the whole energy exchange from the $u_n$ field to $B_n$. Negative values of $S_p$ means that energy is taken from $u_n$.

figure indicates that the dissipative scale is not changed much by the coupling of the velocity field to the polymer field: both the Sabra and SabraP models show a maximum at $k_n$ with $n \sim 15$, which is the dissipative scale. We now address the question how to recapture the same phenomenon in a model involving the velocity field alone but with a scale-dependent effective viscosity. We first reiterate that the field $u_n$ loses energy in favor of the field $B_n$. Using Eq. (5) we can measure the energy transfer from $u_n$ to $B_n$ using the quantity

$$S_p \equiv \sum_n s_p(k_n) \equiv \frac{\nu_p P(B)}{3\tau} \mathrm{Re}\{i\Sigma_n u_n^* \Phi_n(B,B)\}. \qquad (10)$$

This function measures the exchange between the fluid kinetic energy and the "polymer" or "elastic" energy. In Fig. 5 we show a snapshot of the dependence of the function $S_p$ on time. The point to notice is that $S_p$ is negative for most of the time. The $B_n$ field drains energy from the velocity field, and we therefore can hope to be able to capture its role by an effective viscosity. Note, however, that the dynamics of $S_p$ is strongly intermittent; this feature is common to the shell model and the FENE-P model as observed in the direct numerical simulations of the latter. We cannot hope to capture *all* the temporal complexity with the notion of effective viscosity, since the latter is an average notion. Nevertheless, the essential features will be shown to be reproduced. We will try to capture the effect of $S_p$ in terms of an effective viscosity as follows: using $\langle \ldots \rangle$ for the (time) average, we introduce the scale dependent effective viscosity $\nu_e(k_n)$ as

$$\nu_e(k_n) = -\frac{\langle s_p(k_n) \rangle}{k_n^2 e(k_n)}. \qquad (11)$$

The quantity $\nu_e(k_n)$ is shown in Fig. 6; its maximum is reached at $k_n$ with $n \sim 6$–$7$, a wave number which is not yet in the dissipative range. It is important to stress that $\nu_e(k_n)$ is obtained by averaging over a complex and intermittent dynamical behavior of the viscoelastic shell model. It is therefore not obvious that the main characteristics of drag reduction can be obtained by simply replacing the viscoelastic terms $\Phi_n(B,B)$ by a scale-dependent effective viscosity. We demonstrate that this is possible by using now the Sabra model with an extra viscous term given by $\nu_e(k_n)k_n^2 u_n$. The

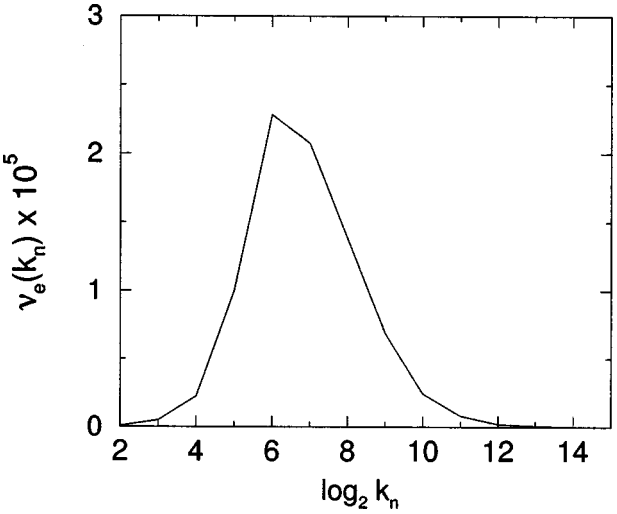


FIG. 6. The values of the eddy viscosity $\nu_e(k_n)$ defined in Eq. (11) for $P(B)=1$. Note that this quantity rises rapidly in the vicinity of the Lumley scale.

new viscous term replaces, on the average, the effect of viscoelastic terms proportional to $\Phi_n(B,B)$. The equations of motion read

$$\frac{du_n}{dt} = \frac{i}{3}\Phi_n(u,u) - \nu_e(k_n)k_n^2 u_n - \nu_s k_n^2 u_n + F_n. \qquad (12)$$

We do not expect that $\nu_e(k_n)$ in the *dynamics* of the Sabra model, as proposed in Eq. (12), will be exactly the object measured on the average defined in Eq. (11). We clearly must keep the functional dependence of $\nu_e$ on $k_n$, but we can allow a factor of proportionally that will take care of the difference between the dynamical intermittent behavior and the average behavior. We will therefore use the form $\alpha\nu_e(k_n)$, where $\alpha$ is a constant that can be optimized to achieve a close correspondence between the two-field model and the effective one-field model. For $\alpha=0$ it reduces to the Sabra model without effective viscosity. We simulated the Sabra model with the effective viscosity [Eq. (12)] for different values of $\alpha$ in the range $(0,1)$. Drag reduction was found in all cases. For $\alpha=0.3$ the energy spectrum on the large scales, the most relevant ones for drag reduction to occur, turns out to be very close to the SabraP model *with the viscoelastic terms*. In Fig. 7 we show the energy spectrum of the SabraP model and the energy spectrum of the Sabra model with effective viscosity for $\alpha=0.3$. It is interesting to understand whether one can compute the value of $\nu_e(k_n)$ by using some *a priori* theoretical estimates. We argue that this is possible by the following considerations. $\nu_e(k_n)$ should reach its maximum near the scale $k_c$. Next, let us define $\nu_e^M$ as the maximum value of $\nu_e(k_n)$. One can compute $\nu_e^M$ by the requirement that the Kolmogorov scale $k_M$, computed by using $\epsilon$ (the constant energy input) and $\nu_e^M$, must be as large as possible, although smaller than $k_c$. Thus, for $k_n > k_c$ and $k_n < k_c$, the detailed shape of $\nu_e(k_n)$ is not crucial to affect the dynamics of the system, i.e., the detailed functional dependence of $\nu_e(k)$ on $k_n$ is not relevant as long as the region where $\nu_e(k) \neq 0$ is not too narrow

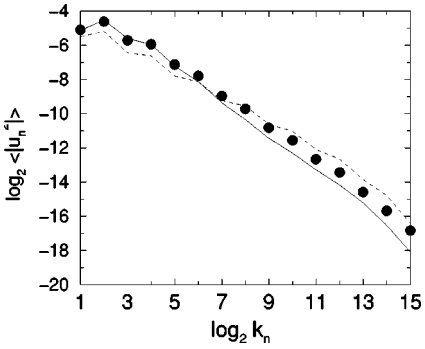


FIG. 7. The energy spectrum of the SabraP model (solid line) as compared with the energy spectrum of the Sabra model with the effective viscosity and $\alpha=0.3$ (symbols) and the Sabra model without effective viscosity (dashed line).

about the scale $k_c$. These arguments will be the subject for future investigations.

In order to check that the results shown in Fig. 7 are due to a *scale-dependent* dissipation, we have defined a *scale-independent viscosity* $\nu_A$ as

$$\nu_A = \frac{\langle S_p \rangle}{\Sigma_n k_n^2 e(k_n)}. \tag{13}$$

The definition of $\nu_A$ is similar to that given in Eq. (11), i.e., $\nu_A$ is defined such that, by adding a viscous term $\nu_A k_n^2 u_n$ to the Sabra model, the system *on the average* is losing the same amount of energy as in the case of viscoelastic flows. It turns out that in our case $\nu_A \sim 2.5\times 10^{-7}$. By using this value for $\nu_A$ we have numerically integrated the Sabra model by adding a new viscosity equal to $\nu_A$, namely

$$\frac{du_n}{dt} = \frac{i}{3}\Phi_n(u,u) - \nu_A k_n^2 u_n - \nu_s k_n^2 u_n + F_n. \tag{14}$$

The corresponding energy spectrum is shown in Fig. 8 together with the energy spectrum for the Sabra model (viscosity $\nu_s$) and the Sabra model with the effective viscosity $0.3\nu_e(k_n)$. As one can clearly see, an increase of the dissipation for all scales does not result in a drag reduction. Finally, we have computed the energy flux of the Sabra model with effective dissipation and compared it against the energy flux of the SabraP model. This comparison is exhibited in Fig. 9 where the solid line corresponds to the SabraP model and the symbols correspond to the Sabra model with effective dissipation $0.3\nu_e(k_n)$. The two energy fluxes are equal in the inertial range up to wave number $k_n$ with $n\sim 7$.

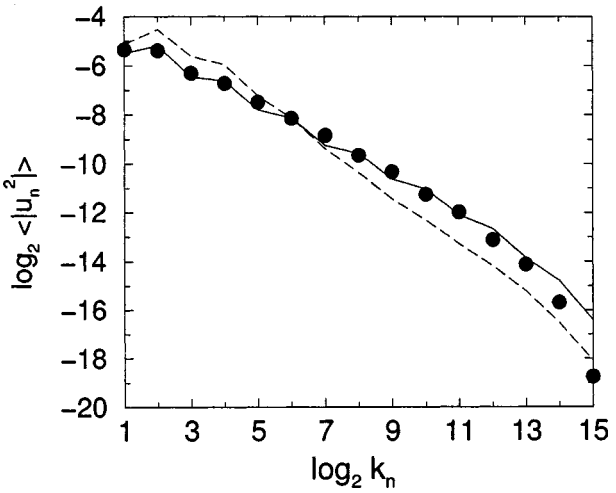


FIG. 8. Energy spectrum of the Sabra model for $\nu_s$ (line), the Sabra model with increased viscosity $\nu_A$ (symbols), and for the Sabra model with an effective viscosity $0.3\nu_e(k_n)$ (dashed line).

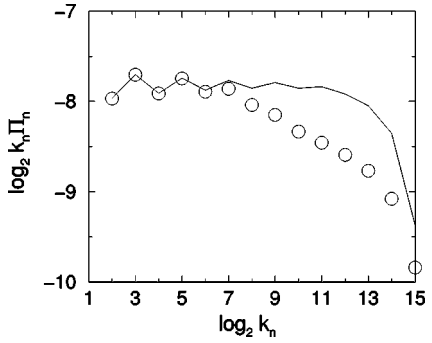


FIG. 9. Energy flux computed for the SabraP model (solid line) and the Sabra model with effective viscosity (symbols).

The results illustrated so far support the conclusion that a scale-dependent effective viscosity is able to reproduce most of the dynamics of the viscoelastic terms and, in particular, the phenomenon of drag reduction. Let us remark once more, that it is the *scale dependence* of the effective viscosity which is able to properly reproduce the drag reduction. It is worthwhile to explain the mechanism of the action of the scale-dependent viscosity, to understand its similarity to the action of the polymers. For fixed energy input, as in our case, drag reduction is shown as an increase of the rms fluctuations at scales larger than the Lumley scale. The scale-dependent effective viscosity increases the viscous terms $k_n^2 u_n$ in a particular range of scales, say for $n_c < n < n_2$, where $n_c = \log_2(k_c)$. The energy flux $\Pi_n$ in the system is given by the third order correlation function $\Pi_n \sim \langle u_{n-1}^* u_n^* u_{n+1} \rangle$. As shown in Fig. 9, we can safely assert that the energy flux does not change for $n < n_c$. The increase of viscosity at $n=n_c$ produces a decrease of the energy at scale $n_c$. Thus, we expect $u_{n_c}$ to decrease with respect to the value observed in the Newtonian case. Since $\Pi_n$ is not affected by the increase of the viscosity at $n=n_c$, we must conclude that the quantity $u_{n-1}u_n$ should increase while $u_{n_c}$ decreases. This is the origin of the tilt in the spectrum and the increase of $u_n$ spectrum in the vicinity of $n_c$. From a physical point of view, this picture is not different from the one discussed in Ref. [9] where a similar explanation for the drag reduction was invoked. Note that all that we need for the phenomenon to occur is that the increase in viscosity should start at the right scale. This scale is equivalent to the Lumley scale whose role in the viscoelastic case has been already emphasized.

Finally, we discuss the effect of changing the concentration on the effective viscosity. When $\langle P(B) \rangle > 1$ the effective viscosity depends on the Peterlin function, which in turn depends on the concentration $c$ and on the relaxation time $\tau$, cf.

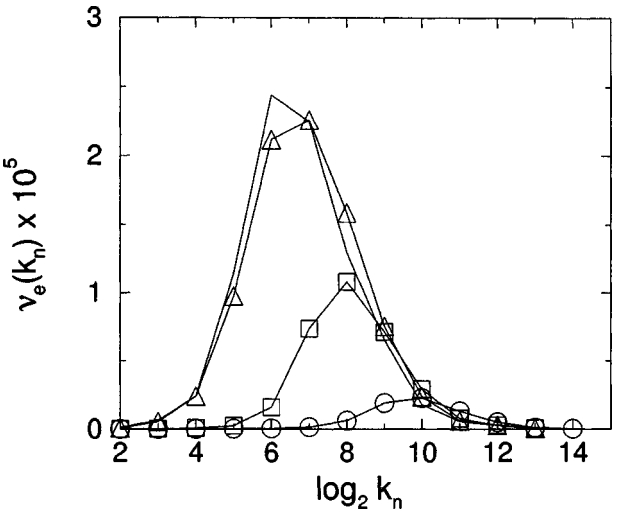


FIG. 10. Effective viscosity for varying the concentration: $c = 10^{-2}$ (circles), $c = 10^{-1}$ (squares), $c = 10$ (triangles), and $c = 100$ (line).

Eq. (11). Figure 10 displays the effective viscosity as a function of $k_n$ for four values of the concentration, $c = 10^{-2}$, $10^{-1}$, 10, and 100. As the concentration decreases, the effective viscosity decreases, and its peak migrates to higher values of $k_n$. This migration is simply due to the change in the Lumley scale, cf. Eq. (9). The decrease in the effective viscosity is due to the increase in $\langle P(B) \rangle$ shown in Fig. 3. Needless to say, these changes in the effective viscosity decrease the effect of drag reduction, as seen in experiments and simulations: only large concentrations agree with the MDR asymptote.

## IV. THE LIMIT OF LARGE SYSTEM SIZE

In this section we want to discuss the limit $k_0 \to 0$ while keeping fixed the scale and the shape of the effective viscosity. In other words, we study $k_0 \to 0$ for fixed value of the Lumley scale $k_c$. Note that we take $k_c$ much smaller than the dissipative scale and we keep constant the rate of energy input $\epsilon$.

The discussion simplifies by considering the other typical scale in our system, which is the Taylor microscale $\lambda_T$:

$$\lambda_T \equiv \sqrt{\frac{\Sigma_n \langle |u_n|^2 \rangle}{\Sigma k_n^2 |u_n|^2}}. \tag{15}$$

In Ref. [9] it was shown that the conditions are optimal for drag reduction in our shell model when a dimensionless parameter, $\mu \equiv \lambda_T k_c$, is of the order of unity. On the other hand drag reduction is lost when $\mu \gg 1$ or $\mu \ll 1$. Obviously, when $k_0 \to 0$ the overall kinetic energy increases as $k_0^{-2/3}$ while the denominator in Eq. (15) remains unchanged, being dominated by the viscous scale. Thus, $k_0 \to 0$ leads to $\lambda_T \to \infty$, and we expect to lose drag reduction in that limit (for a fixed value of $k_c$). This conclusion is supported by the results shown in Fig. 11, where we plot the ratio between the kinetic energy with the effective viscosity and the Newtonian kinetic energy for $L \equiv k_0^{-1} \to \infty$. The case $L = 1$ corresponds to the

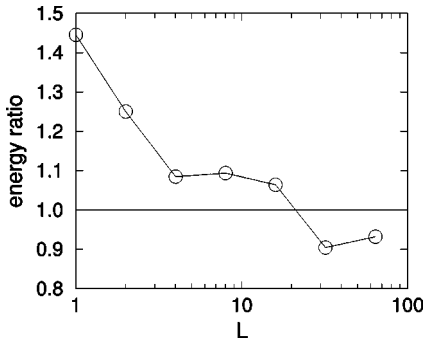


FIG. 11. Ratio of the kinetic energy for the Sabra model with scale dependent viscosity and the kinetic energy of ths Sabra model with fixed kinematic viscosity, for different values of $L \equiv k_0^{-1}$. Note that for drag reduction to occurs the ratio must be larger than 1. The scale of the maximum in the scale dependent viscosity is kept fixed while $L \to \infty$.

previous sections. Note that for $L$ large enough, the system exhibits drag enhancement. Physically, for very large values of $k_c/k_0$ the effective dissipation is just increasing the overall viscosity in the system and, therefore, no drag reduction can be observed. For drag reduction to occur we must have the Lumley scale close to energy containing scales. Note, however, that "close" in our case means $k_c \sim 50-100$ larger than the integral scale $k_0$.

It is interesting to compare our findings, which pertain to homogeneous systems, to drag reduction in turbulent boundary layers. The elastic layer in such flows (between the viscous layer and the Newtonian plug) has the peculiar distinction that $y$, the distance from the wall, becomes the only important scale in the problem. It is both the energy containing scale and the Lumley scale at the same time. The former is clear; at distance $y$ from the wall the most energetic eddies are of size $y$. The latter needs a bit of theory, and this is provided in Ref. [13]. The upshot of the analysis there is that in the elastic layer the kinetic energy $K(y)$ scales like $K(y) \sim y^2/\tau^2$. Thus, the Lumley scale is also $y$. Accordingly, the phenomenon of drag reduction is totally indifferent to the physical size of the channel (or pipe). As long as the conditions for drag reduction hold at distance $y$ from the wall, drag reduction will occur and will have a persistent effect on the mean flow independently of the outer scale. Eventually, when $y$ is large enough, $K(y)$ may stop growing like $y^2$, the Lumley scale decreases, and we observe crossover back to the Newtonian log layer, albeit shifted to a larger value of a mean velocity profile.

In summary, drag reduction phenomena in homogeneous and wall bounded flows have a lot in common even though the effect disappears in the former when the system size goes to infinity. The essential physics is the proximity of the Lumley scale to the energy containing scales, which allows an effective interaction between the polymer dynamics and the hydrodynamic modes.

## V. CONCLUSIONS

The work presented in this paper supports two conclusions. First, we demonstrated that drag reduction by poly-

mers can be represented in terms of an effective scale dependent viscosity. One can use a theory in which two fields are explicitly present, i.e., the velocity field and the polymer field. Then the viscosity remains Newtonian, and the polymer conformation tensor acts as the additional sink of energy at the intermediate scales which are larger than the viscous scales but smaller than the Lumley scale. We can construct, however, effective models in which only the velocity field is present, and replace the polymer field by an effective viscosity. This effective viscosity will be different from the Newtonian one at the crucial scales at which the polymers are active, i.e., scales larger than the dissipative scales but smaller than the Lumley scale. With a properly chosen effective viscosity we can reproduce the results of the two-field theory qualitatively and even semiquantitatively. Having done so, we reach a unified discussion of drag reduction by polymers in homogeneous and wall bounded flows. It is worth pointing out, however, that the unified discussion is deeper than the device of unified viscosity. Superficially drag reduction in homogeneous and wall bounded turbulence appear very different. In the former there is no mean flow and drag reduction appears as an increase of the rms fluctuations of the large scales. In the latter drag reduction means the increase of the mean flow velocity. Nevertheless in essence the phenomenon of drag reduction in homogeneous and wall bounded flows is basically the same: the polymers act to reduce the gradients at the intermediate scales. They partly laminarize the flow at the intermediate scales, and this allows the largest scales to attain higher rms fluctuation levels (in homogeneous flows) or higher mean velocity (in wall bounded flows). To understand this further recall that for laminar flows the drag is a strongly decaying function of Re. Once turbulence sets in, the dramatic increase in eddy viscosity contributes to a drag which is much larger than the one obtained in a hypothetical laminar flow with the same value of Re. The addition of polymers allows one to bring the drag closer to the hypothetical low laminar value, and this is done by reducing the turbulence level at intermediate scales. Whether one prefers to describe the quantitative aspects of this phenomenon using explicitly the polymer field or by employing an effective viscosity depends to a large extent on one's goals. We expect that the concept of effective viscosity will be found equally useful in discussing drag reduction in other situations, for example when microbubbles are used instead of polymers. The quantitative aspects of such a description need, however, to be worked out case by case, and this is our program for the near future.

## ACKNOWLEDGMENTS

This work was supported in part by the European Commission under a TMR grant, the U.S.-Israel Binational Science Foundation, and the Naftali and Anna Backenroth-Bronicki Fund for Research in Chaos and Complexity. E.S.C.C. was supported by a grant of the Research Grant Council of Hong Kong (Ref. No. CUHK 400304P).

[1] K. R. Sreenivasan and C. M. White, J. Fluid Mech. **409**, 149 (2000).
[2] J. L. Lumley, Annu. Rev. Fluid Mech. **1**, 367 (1969).
[3] P. S. Virk, AIChE J. **21**, 625 (1975).
[4] P.-G. de Gennes, *Introduction to Polymer Dynamics* (Cambridge University Press, Cambridge, 1990).
[5] B. A. Toms, *Proc. 1st Intl. Congress on Rheology* (North-Holland, Amsterdam, 1949), Vol. 2, p. 135.
[6] J. M. J. de Toonder, M. A. Hulsen, G. D. C. Kuiken, and F. T. M. Nieuwstadt, J. Fluid Mech. **337**, 193 (1997).
[7] C. D. Dimitropoulos, R. Sureshdumar, and A. N. Beris, J. Non-Newtonian Fluid Mech. **79**, 433 (1998).
[8] E. de Angelis, C. M. Casciola, and R. Piva, Comput. Fluid Dyn. J. **9**, 1 (2000).
[9] R. Benzi, E. De Angelis, R. Govindarajan, and I. Procaccia, Phys. Rev. E **68**, 016308 (2003).
[10] R. Benzi and I. Procaccia, Phys. Rev. E **68**, 025303 (2003).
[11] R. Benzi, E. Ching, N. Horesh, and I. Procaccia, Phys. Rev. Lett. **92**, 078302 (2004).
[12] E. De Angelis, C. M. Casciola, V. S. L'vov, R. Piva, and I. Procaccia, Phys. Rev. E **67**, 056312 (2003).
[13] V. S. L'vov, A. Pomyalov, I. Procaccia, and V. Tiberkevych, Phys. Rev. Lett. **92**, 244503 (2004).
[14] R. Govindarajan, V. S. L'vov, and I. Procaccia, Phys. Rev. Lett. **87**, 174501 (2001).
[15] R. Govindarajan, V. S. L'vov, I. Procaccia, and A. Sameen, Phys. Rev. E **67**, 026310 (2003).
[16] S. B. Pope, *Turbulent Flows* (Cambridge University Press, Cambridge, 2000).
[17] M. V. Zagarola and A. J. Smits, Phys. Rev. Lett. **78**, 239 (1997).
[18] R. B. Bird, C. F. Curtiss, R. C. Armstrong, and O. Hassager, *Dynamics of Polymeric Fluids* (Wiley, New York, 1987), Vol. 2.
[19] A. N. Beris and B. J. Edwards, *Thermodynamics of Flowing Systems with Internal Microstructure* (Oxford University Press, New York, 1994).